Supplementary Information

Fluorescent polymer cubosomes and hexosomes with aggregation-induced emission

Hui Chen,[a] Yujiao Fan,[a] Nian Zhang,[a,b] Sylvain Trépout,[c] Bergam Ptissam,[c] Annie Brûlet,[d] Ben Zhong Tang,[e] Min-Hui Li[a]*

[a] Chimie ParisTech, PSL Université Paris, CNRS, Institut de Recherche de Chimie Paris, UMR8247, 11 rue Pierre et Marie Curie, 75005 Paris, France.

[b] Beijing Advanced Innovation Center for Soft Matter Science and Engineering, Beijing University of Chemical Technology, 15 North Third Ring Road, Chaoyang District, 100029 Beijing, China.

[c] Institut Curie, Université Paris-Saclay, Inserm US43, CNRS UMS2016, Centre Universitaire, Bât. 101B-110-111-112, Rue Henri Becquerel, CS 90030, 91401 ORSAY Cedex, France.

[d] Laboratoire Léon Brillouin, Université Paris-Saclay, UMR12 CEA-CNRS, CEA Saclay, 91191 Gif sur Yvette cedex, France.

[e] Department of Chemistry, Hong Kong University of Science and Technology, Clear Water Bay, Kowloon, Hong Kong, China.

Email : min-hui.li@chimieparistech.psl.eu

Contents

1. Materials

Diphenylmethane (99%, Alfa Aesar), 4-methoxybenzophenone (97%, Acros), *n*-butyllithium (2.5 M in hexane, Sigma-Aldrich), *p*-toluenesulfonic acid monohydrate (97%, Alfa Aesar), boron tribromide (BBr_3, 1.0 M in dichloromethane, Sigma-Aldrich), 3-bromo-1-propanol (97%, Alfa Aesar), potassium carbonate (K_2CO_3, 99%, Sigma-Aldrich), methacryloyl chloride (97%, Sigma-Aldrich), triethylamine (99%, Alfa Aesar), *n*-dodecylthiol (98%, Sigma-Aldrich), sodium hydride (60% dispersion in mineral oil, Sigma-Aldrich), carbon disulfide (99%, Sigma-Aldrich), iodine (99%, Sigma-Aldrich), 4,4'-azobis(4-cyanopentanoic acid) (98%, Alfa Aesar), *N,N'*-dicyclohexylcarbodiimide (99%, Sigma-Aldrich) and 4-(dimethylamino)pyridine (99%, Sigma-Aldrich) were used as received. Poly(ethylene glycol) monomethyl ether (mPEG-OH, M_n = 2000 Da) was purchased from Fluka and purified by precipitation in diethyl ether for three times before use. 2,2'-Azobis(isobutyronitrile) (AIBN) was recrystallized from ethanol for three times before use.

2. Methods

Cell viability assay

The toxicity of cubosomes and hexosomes has been tested on two different cell lines with several cubosomes and hexosomes concentrations. Malignant human melanoma cells A375M were cultured in RPMI medium supplemented with 10% fetal bovine serum (FBS) and 1% streptavidin/penicillin. Adenocarcinomic human alveolar basal epithelial lung cells A549 were cultured in DMEM Glutamax medium supplemented with 10% fetal bovine serum (FBS) and 1% streptavidin/penicillin.

Proliferation assays were performed using an IncuCyte™ live-cell Imaging apparatus. This system measures cell growth in real time and automatically calculates the phase object-based confluence at each time point. For each test condition, about 800 cells (counted with a Malassez cell) were seeded into a well of a 96-well plate, with 200 µL of medium, and incubated in a humidified atmosphere of 5% CO_2 at 37 °C. After 24h, giving enough time for the cells to adhere to the plate, the medium of each well was changed with 200 µL of medium containing different concentrations of hexosomes or cubosomes (15 µg/mL, 50 µg/mL, 250 µg/mL and

500 μg/mL) with propidium iodide (PI) at concentration of 0.3 μg/mL. Control cells were only treated with PI. PI was used to monitor cell death. Overall, 9 conditions were tested (including the control) for each cell line. Phase-contrast images and fluorescence images (PI $\lambda_{excitation}$ 535 nm / $\lambda_{emission}$ 617 nm) were acquired with a 4X objective in the Incucyte in real time every 3 hours, from day 0 to day 4 after treatment. The "confluence mask" was selected for the recognition of living cells so that the cell confluence could be determined over time by analyzing the acquired images. The "cell death mask" was selected for the recognition of cells that emitted PI at 617 nm (red). Each experimental condition was repeated 3 times.

3. Instruments

Nuclear Magnetic Resonance (NMR)

^{1}H NMR and ^{13}C NMR spectra were recorded on Bruker Avance III HD 400 MHz spectrometer at 298 K. Deuterated chloroform ($CDCl_3$) was used as the solvent. NMR chemical shifts were recorded in parts per million referenced to the residual solvent proton (δ = 7.26 ppm) for ^{1}H NMR and carbon (δ = 77.1 ppm) for ^{13}C NMR.

Size Exclusion Chromatography (SEC)

Molecular weights (MWs) and molecular weight distributions (Đ) were determined by size exclusion chromatography (SEC) which was consisted of a Waters 1515 isocratic high-performance liquid chromatograph pump, two Styragel HR 5E columns and a refractive index (RI) detector. DMF containing 0.01 mol/L LiBr was used as the eluent with a flow rate of 1.0 mL/min at 60 °C. Commercial monodispersed polystyrenes (PS) were used as the calibration standards.

Fluorescence emission spectroscopy

The fluorescence emission spectroscopy characterization was carried out on a FluoroMax spectrofluorometer. Samples were added to a 1cm quartz cuvette with all flanks transparent.

Dynamic light scattering (DLS)

Hydrodynamic diameters (D_h) of the self-assemblies of amphiphilic PEG-*b*-PTPEMA block copolymers and their size distributions in deionized water were measured at 25 °C by

dynamic light scattering (DLS, Malvern zetasizer 3000HS, UK) with a 633 nm laser. All measurements were performed with a 90° scattering angle. The sample solution in the scattering cell was equilibrated for 2 min before measurement.

Cryo-electron microscopy (Cryo-EM). Morphologies of the copolymer colloids were characterized by cryo-EM. Images were acquired on a JEOL 2200FS energy-filtered (20 eV) field emission gun electron microscope operating at 200 kV using a Gatan US1000 ssCCD 2048 × 2048 pixels. Samples were prepared by deposition of 5 μL sample solution onto a 200 mesh holey carbon copper grid (Ted Pella Inc., U.S.A.) and the samples were plunge-frozen in liquid ethane cooled down at liquid nitrogen temperature using a Leica EM-CPC.

Small-angle X-ray scattering (SAXS). SAXS experiments were carried out on the Xeuss 2.0 apparatus of Laboratoire Léon Brillouin installed in the SWAXS Lab (CEA Saclay, France). The instrument uses a micro-focused Cu Kα source (wavelength of 1.54 Å, 8 keV) and a Pilatus3 1M detector (Dectris, Switzerland). One configuration was chosen to cover the broad q range, from 0.09 to 4 nm^{-1}, with the sample to detector distance set to 1.18m, a collimated beam size of 1*1 mm^2 at the entrance and 0.6 × 0.6 mm^2 at the exit distant of about 1.3m. The powder sample was placed in a cell made of two square (5mm*5mm) silicon nitride windows separated by a 1mm-thick spacer. The thickness of each window was 200 nm. The scattering intensity of the empty cell, bare beam and dark were measured and subtracted from the scattering intensity of the powder sample according to standard protocols (A. Brûlet, D. Lairez, A. Lapp and J.-P. Cotton, *J. Appl. Crystallogr.*, 2007, **40**, 165-177). Since the amount of powder in the beam was not really controlled, intensity is in arbitrary units. SAXS data analyses were described in detail in Supporting Information.

4. Syntheses and characterizations of PEG-*b*-PTPEMA block copolymers

Take the synthesis of PEG_{45}-*b*-$PTPEMA_{16}$ as an example, the typical RAFT polymerization process was as follows: TPEMA (237 mg, 0.5 mmol), mPEG-CTA (60 mg, 0.025 mmol) and AIBN (0.9 mg, 0.005 mmol) were added into a 15 mL Schlenk tube equipped with a Teflon coated stirring bar. Then 1.5 mL dry THF was added. After the solution was clear, the Schlenk tube was degassed by three freeze-pump-thaw cycles and then immersed into an oil bath of 70

°C. The mixture was stirred at 70 °C for 16 h. The polymerization was terminated by freezing the resultant mixture in liquid nitrogen. The mixture was then poured drop-by-drop into cold isopropanol to precipitate the crude PEG-*b*-PTPEMA. The precipitate was collected by centrifugation. After being re-dissolved in THF and reprecipitated in cold isopropanol twice more and then dried under vacuum at room temperature for 24 h, the pure polymer was obtained as a white solid.

The obtained pure polymer was characterized carefully by NMR (Figure S1), GPC (Figure S2). The ^{1}H NMR spectrum of PEG_{45}-*b*-$PTPEMA_{16}$ copolymer showed all the proton signals of the polymer structure, which confirmed the synthesis of the target block copolymer. The DP of TPEMA units were calculated by comparing the integrated areas of the proton peaks from TPE moiety (peak H_a for TPEMA) and that from the methyl group at the end of PEG block (peak H_b) in the ^{1}H NMR spectrum (Figure S1). M_n of the block copolymer could then be calculated after knowing the DP of each repeating unit on the polymer chain.

Table S1. Synthesis of amphiphilic PEG-*b*-PTPEMA block copolymers

Sample[a]	[mPEG-CTA]/[TPEMA]/[AIBN]	yield	Mn[b]	$Đ$ [c]	$f_{PEG,wt\%}$
PEG_{45}-*b*-$PTPEMA_{16}$	1:20:0.2	65 %	9900	1.10	20%
PEG_{45}-*b*-$PTPEMA_{29}$	1:35:0.2	61 %	17500	1.10	12.3%
PEG_{45}-*b*-$PTPEMA_{42}$	1:50:0.2	60 %	22300	1.11	8.9 %
PEG_{45}-*b*-$PTPEMA_{122}$	1:130:0.2	65 %	60200	1.17	3.3%

[a] All polymer samples were prepared by RAFT using mPEG-CTA (Mn = 2400 Da (NMR), PDI = 1.11) as the macro chain transfer agent in THF at 70 °C. [b] Mn was calculated by ^{1}H NMR; [c] Obtained by SEC in 0.01 M LiBr/DMF, with elution rate at 1 mL/min, PS as standard.

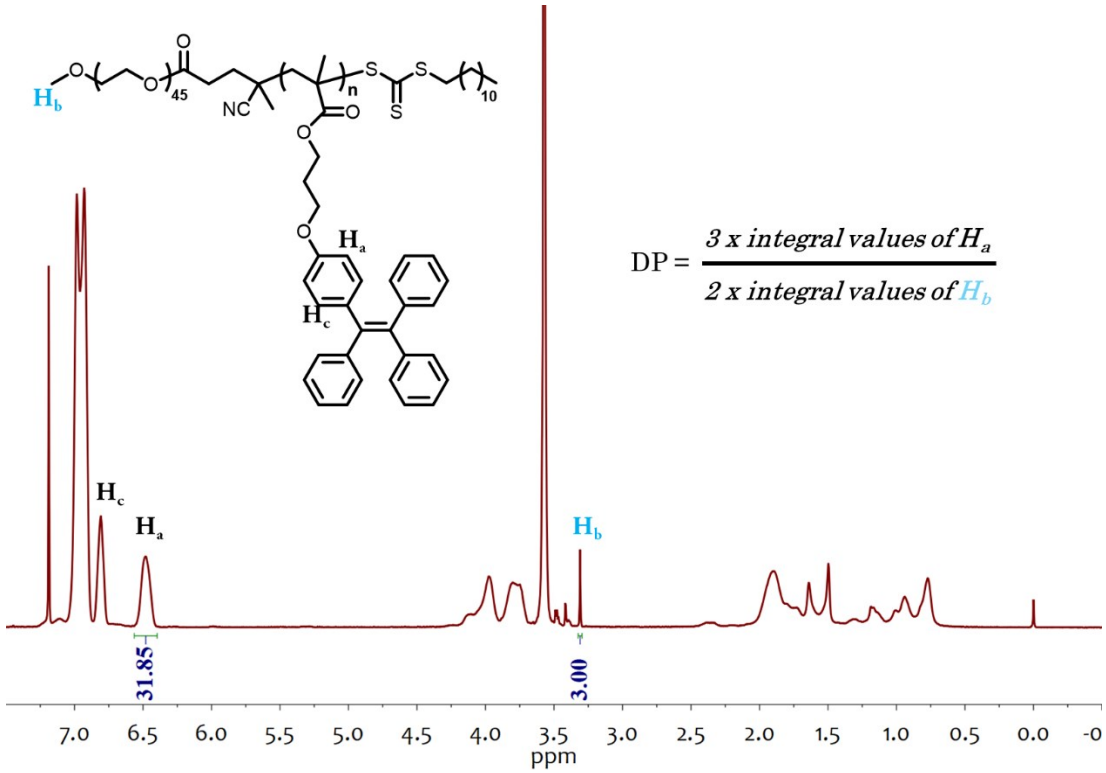

Figure S1. ^{1}H NMR spectrum of PEG_{45}-*b*-$PTPEMA_{16}$ copolymer. ($CDCl_3$, 400 MHz, 298 K).

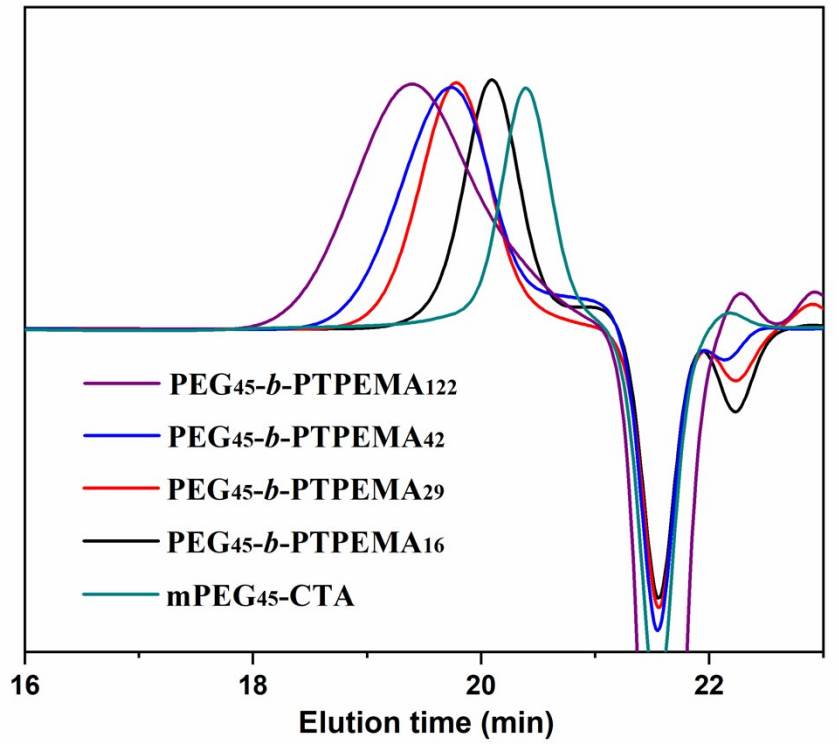

Figure S2. SEC chromatograms of PEG-*b*-PTPEMA copolymers and PEG-macroinitiator ($mPEG_{45}$-CTA). DMF was used as the eluent at a rate of 1mL/min. The signals after 21 min of elution came from the eluent.

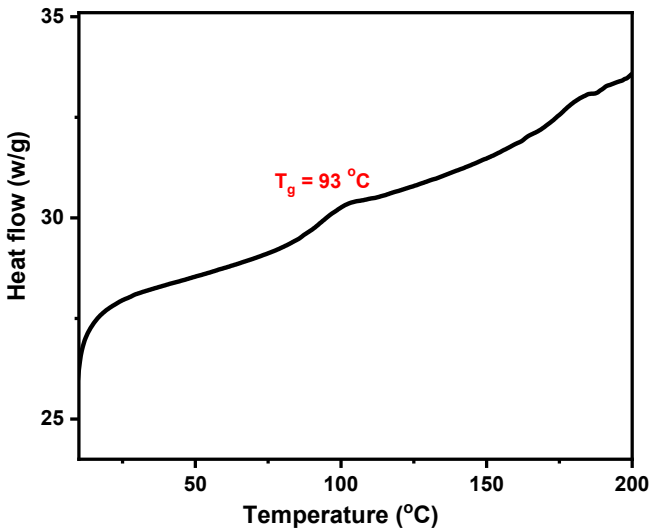

Figure S3. DSC thermogram of PEG_{45}-*b*-$PTPEMA_{122}$ from 0 to 200 ℃ at 10 ℃/min (2^{nd} heating scan).

5. Self-assembly of PEG-*b*-PTPEMA

In the standard procedure, 2.5 mg of PEG-*b*-PTPEMA was dissolved in 2 mL of dioxane. The mixture was stirred for 1h at room temperature. Then 5ml Milli-Q water was added into the organic solvent with the addition rate of 1ml/h under stirring. After the addition, the resultant mixture was dialyzed against a large amount of pure water remove the organic solvent. The aggregates were obtained by centrifugation at 5000 r.p.m. for 10 min, and then dispersed in the water again.

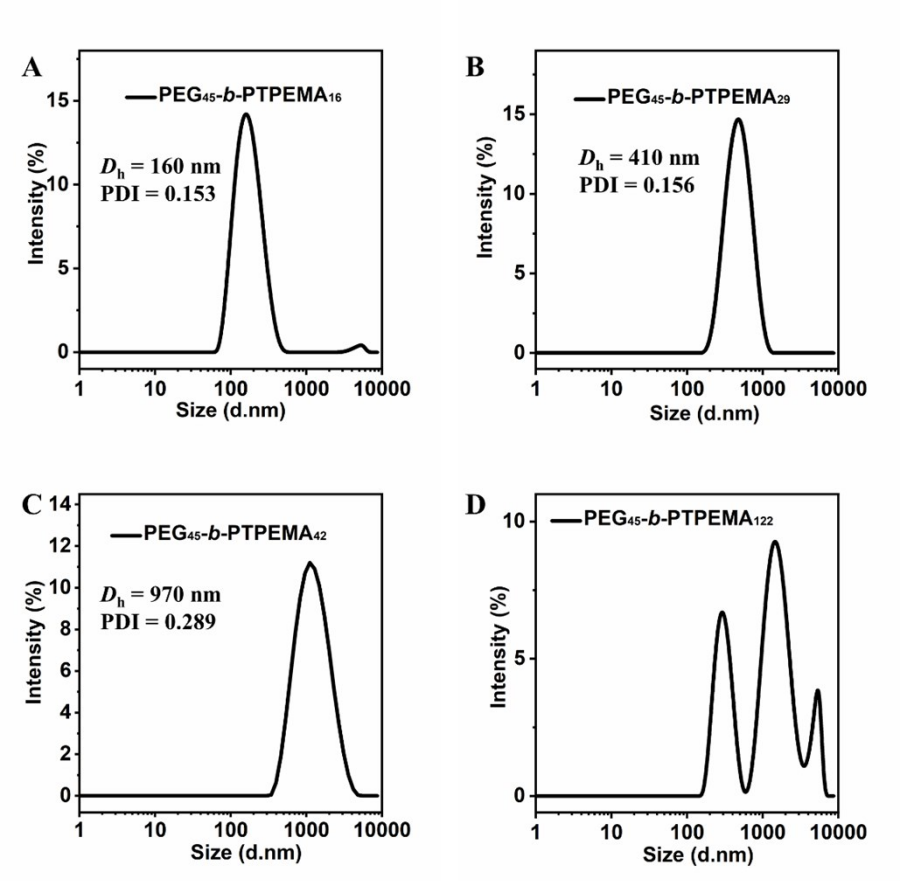

Figure S4. The DLS profiles of self-assemblies formed by PEG_{45}-*b*-$PTPEMA_n$ using dioxane as the cosolvent (initial concentration c_0 = 0.25wt%).

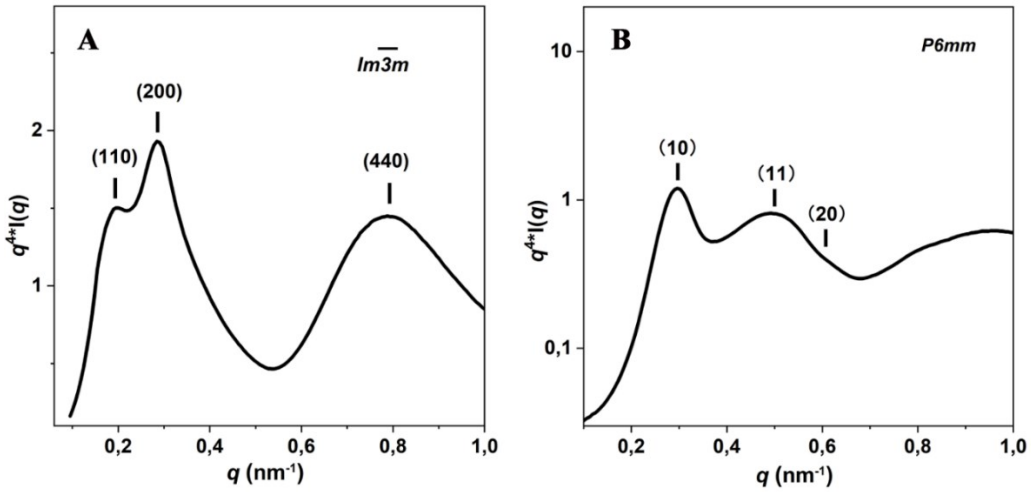

Figure S5. SAXS profiles presented in q^4*I(q) *vs* q for (A) $Im\bar{3}m$ cubosomes of PEG_{45}-*b*-$PTPEMA_{42}$, and (B) hexosomes of PEG_{45}-*b*-$PTPEMA_{122}$. The curve in (A) clearly shows the (110), (200) and (440) reflections of the primitive cubic structure $Im\bar{3}m$, while the curve in (B) shows the (10), (11) and (20) reflections of the hexagonal structure *p6mm*.

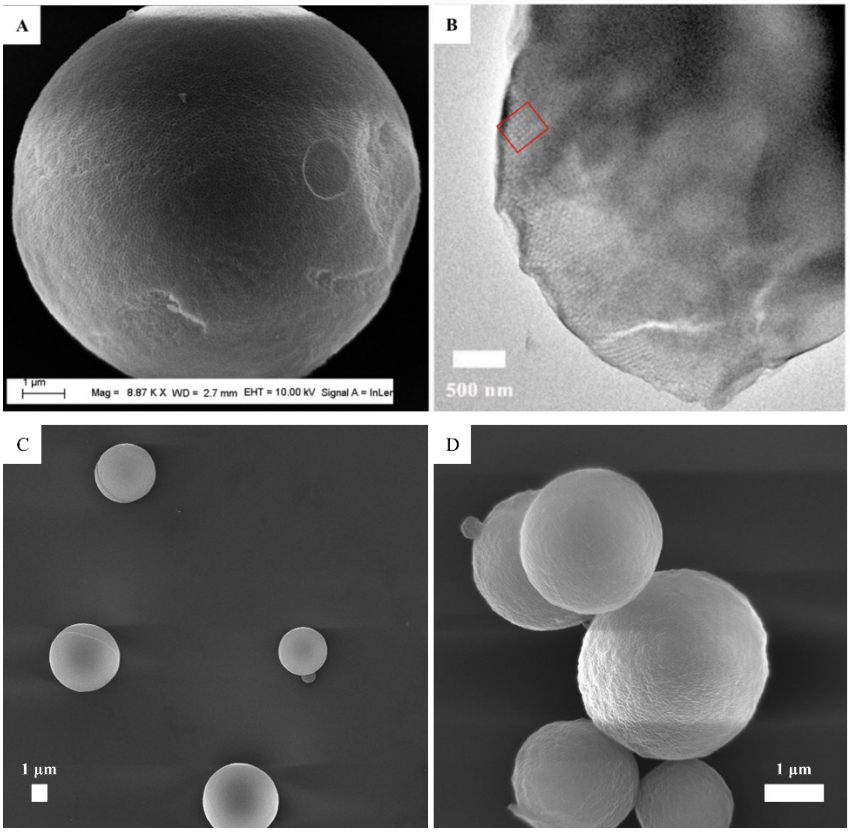

Figure S6. Supplemental results of SEM and TEM images of cubosomes self-assembled by PEG_{45}-*b*-$PTPEMA_{42}$ using dioxane as the cosolvent (initial concentration c_0 = 0.25wt%). B demonstrated the regular internal structures of the crashed cubosome, displaying the typic contrasts of the [100] direction of primitive cubosomes (shown by red rectangle). The dark regions in the cubosome are present because of the inherent large size of the cubosome which cause the scatteration of the electrons before reaching the TEM camera.

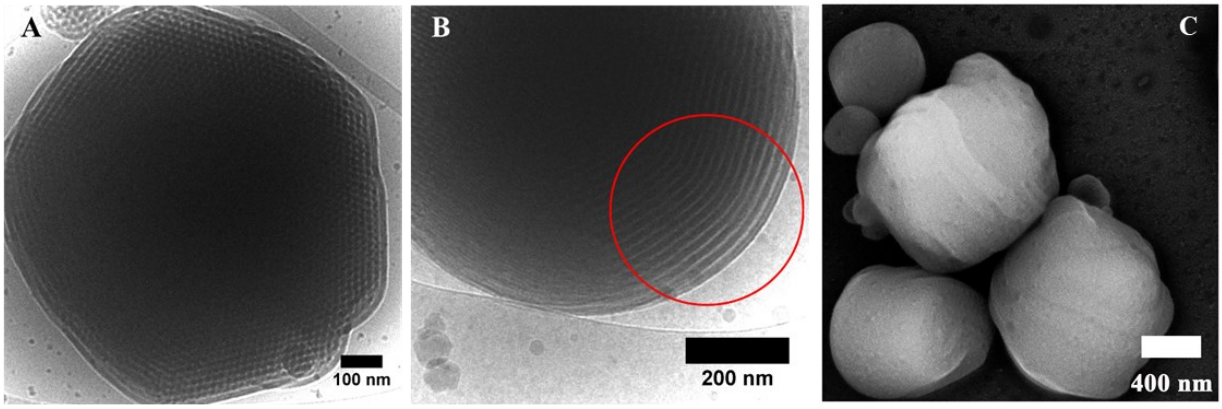

Figure S7. The cryo-EM images (A-B) and SEM (C) of hexosomes formed by PEG_{45}-*b*-$PTPEMA_{122}$ with dioxane as the cosolvent. The red circle in B indicated the hollow hoops in the hexosomes.

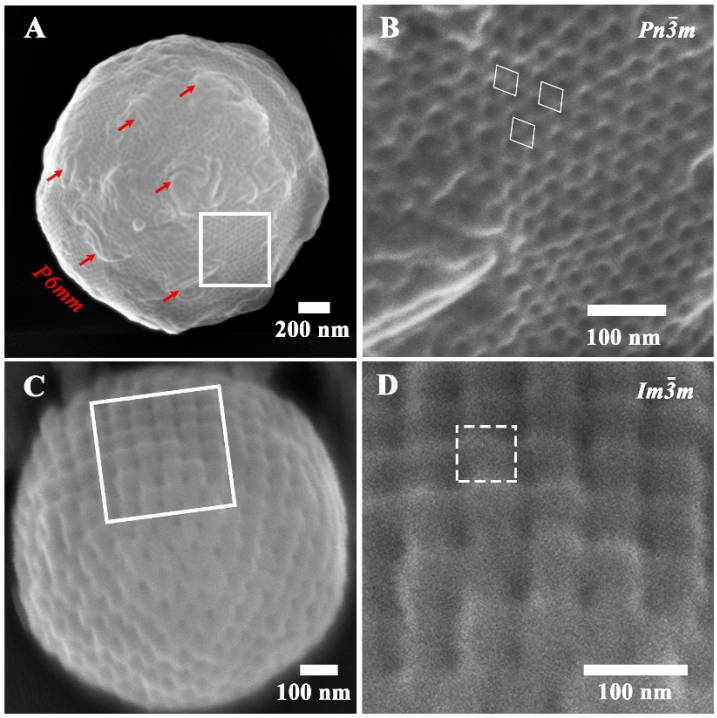

Figure S8. The SEM images of PEG_{45}-*b*-$PTPEMA_{122}$ assemblies using dioxane as cosolvent at the initial polymer concentration of 0.4 wt%. (A) The assemblies with the coexistence of $Pn\bar{3}m$ and *P6mm* structures (The red arrows indicating the cylindrical channels of *P6mm*). (B) The amplification image of the white rectangle part in A, showing the diamond-shaped packing of pores on the surface (indicated by white diamonds). (C) The $Im\bar{3}m$ particles. (D) The amplification image of the white rectangle part in C, showing tetragonal pores on the surface (indicate by dotted line square).

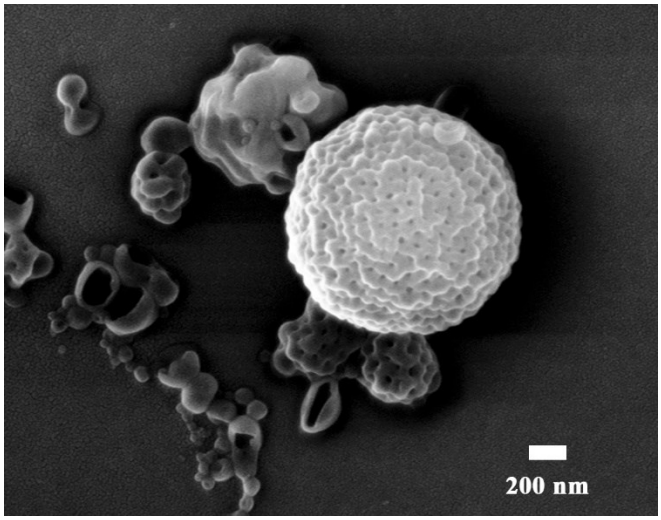

Figure S9. The SEM images of PEG_{45}-*b*-$PTPEMA_{122}$ aggregates using dioxane as cosolvent at

the initial polymer concentration of 2 wt%.

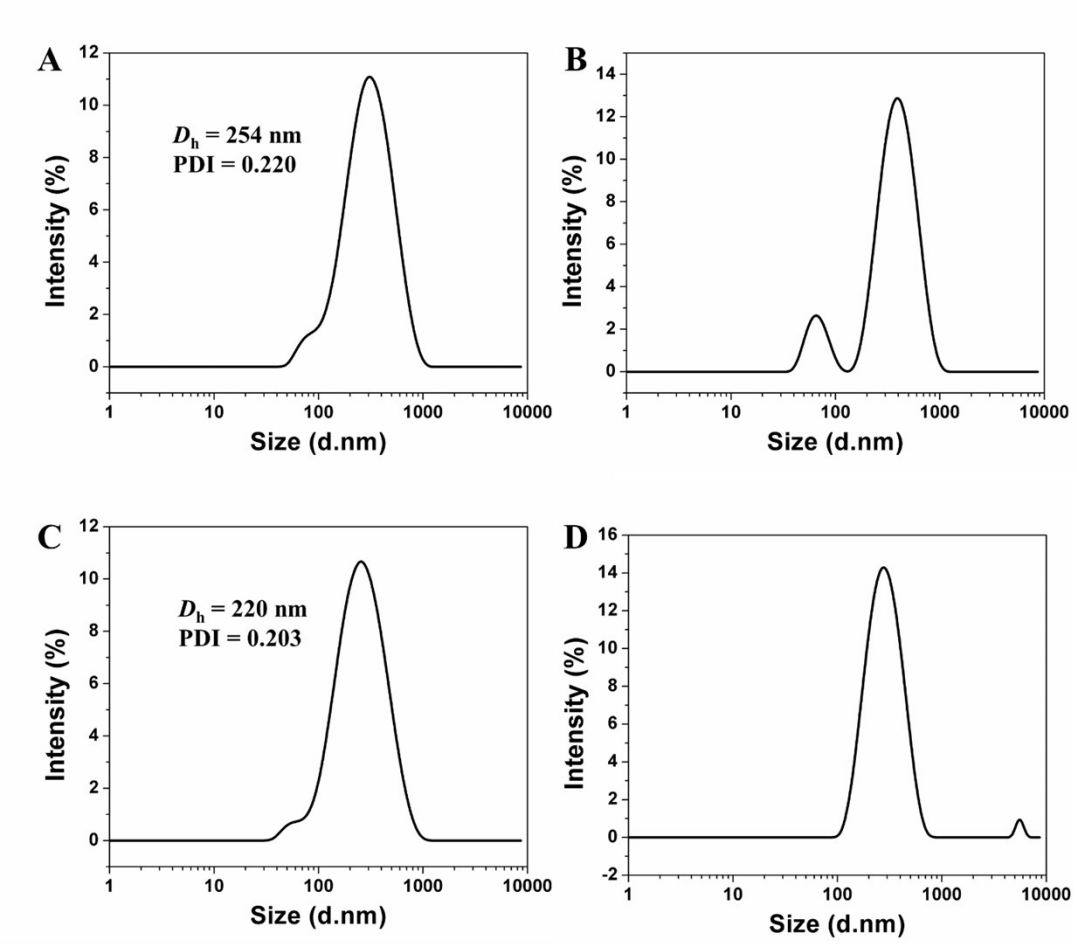

Figure S10. DLS profiles of (A) PEG_{45}-*b*-$PTPEMA_{16}$, (B) PEG_{45}-*b*-$PTPEMA_{29}$, (C) PEG_{45}-*b*-$PTPEMA_{42}$ and (D) PEG_{45}-*b*-$PTPEMA_{122}$ self-assemblies obtained with THF as the cosolvent. (initial concentration c_0 = 0.25wt%).

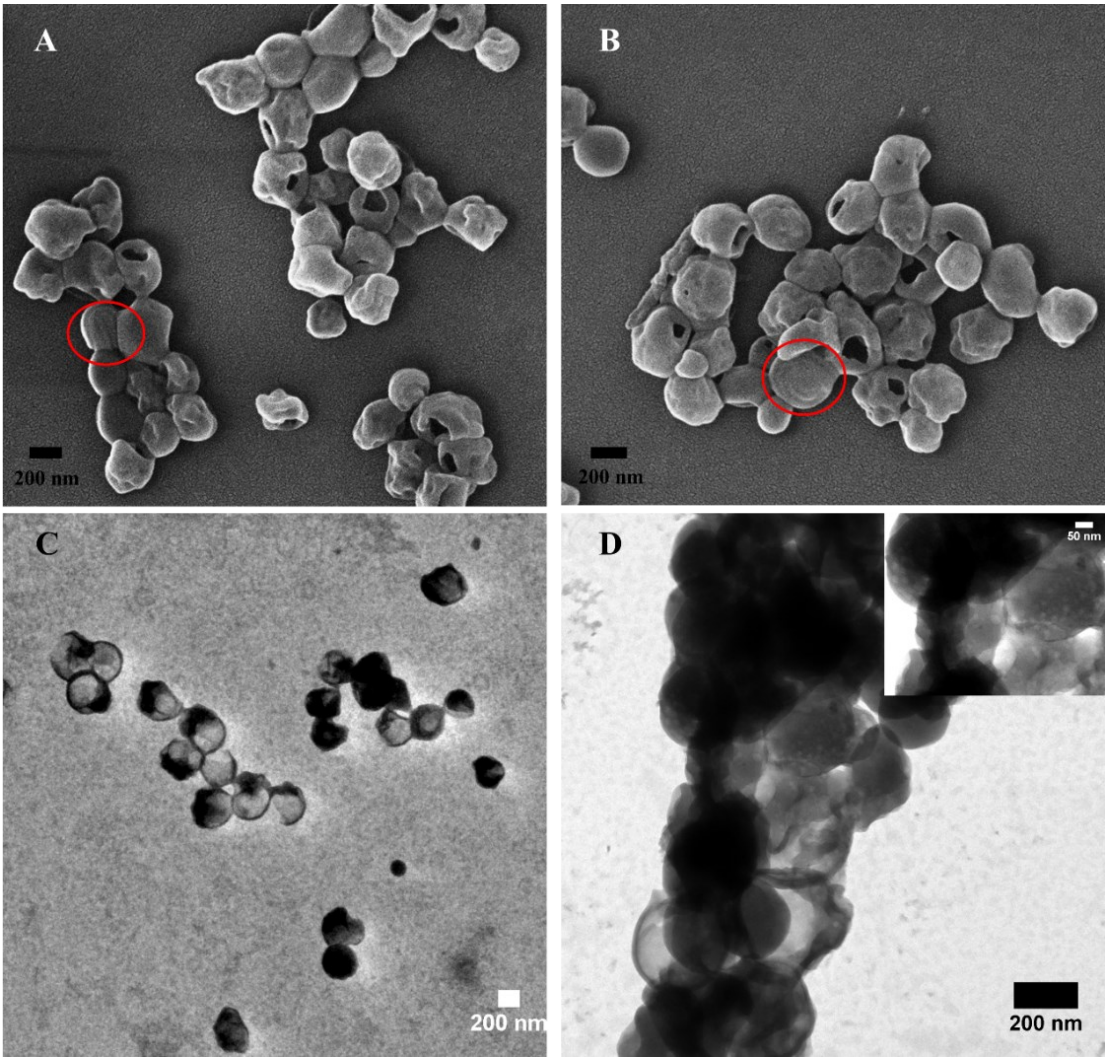

Figure S11. Supplemental results of SEM (A-B) and TEM (C-D) characterizations of aggregates obtained by PEG_{45}-*b*-$PTPEMA_{29}$ in THF/water systems. The red circles in A and B indicate the hexosomes. The inset in D reveal the formation of hexosomes.

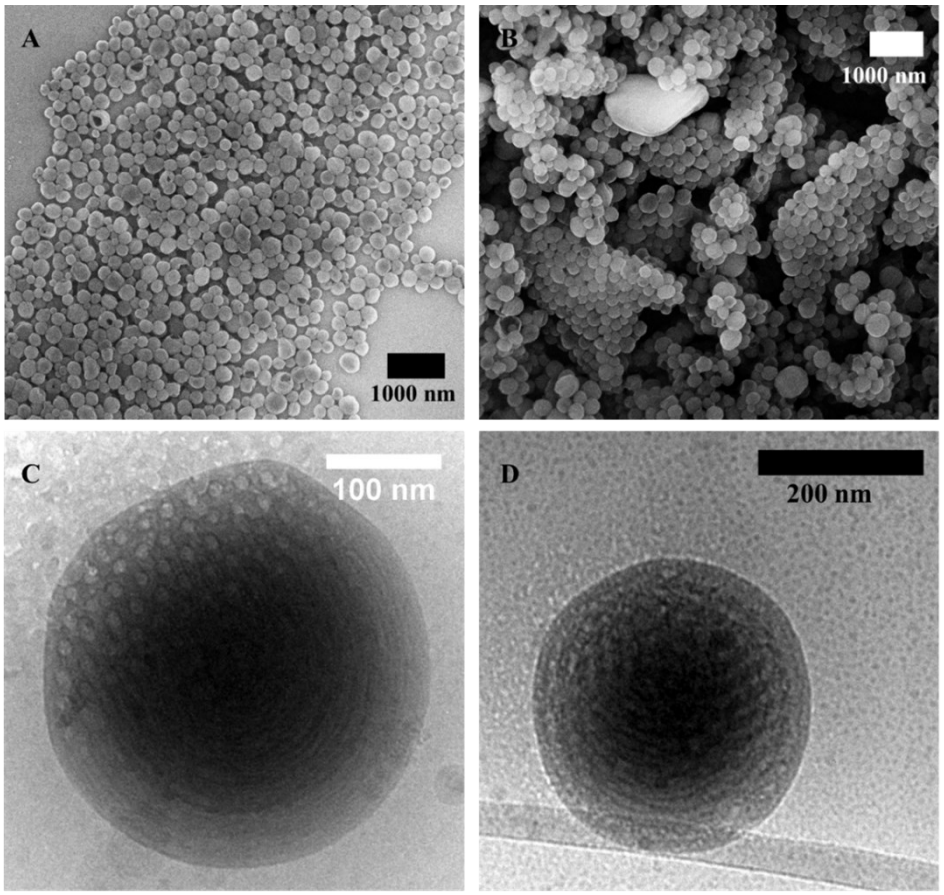

Figure S12. Supplemental results of SEM (A-B), cryo-EM (C-D) characterizations of hexosomes prepared by PEG_{45}-*b*-$PTPEMA_{42}$ in THF/water systems.

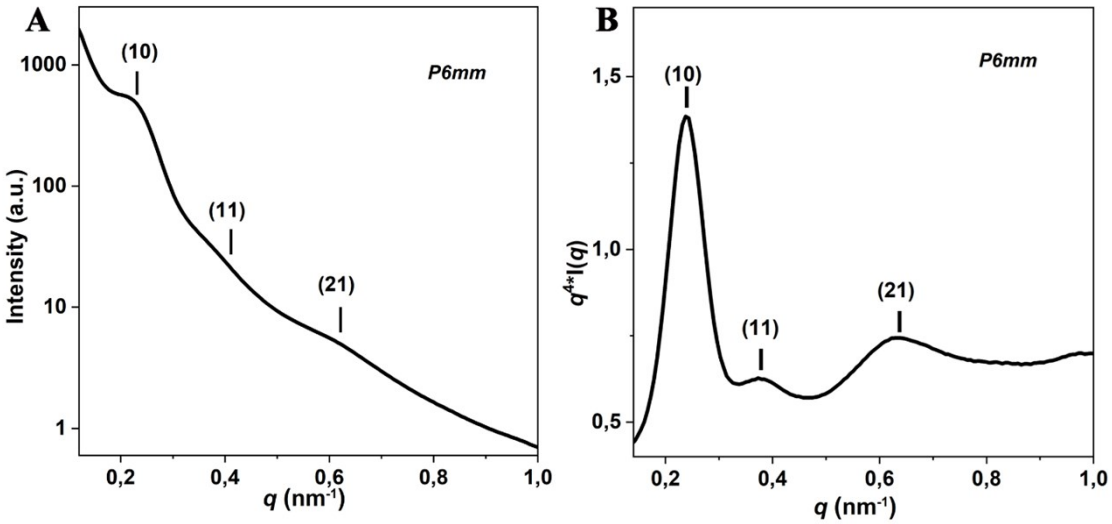

Figure S13. SAXS profiles of hexosomes of PEG_{45}-*b*-$PTPEMA_{42}$ prepared in THF/water system. (A) The curve presented in I(q) *vs* q. (B) The curve presented in q^4* I(q) *vs* q, clearly demonstrating the (10), (11) and (21) reflections of hexagonal structure *p6mm*.

Table S2. Summary of the thickness of the hydrophobic part of bilayer membrane (*e*) for different PEG-*b*-PTPEMA morphologies. [a]

Sample	Dioxane/water system	THF/water system
PEG_{45}-*b*-$PTPEMA_{16}$	8.5±0.5 nm *(polymersomes)*	11.0±0.5 nm *(polymersomes)*
PEG_{45}-*b*-$PTPEMA_{29}$	11.0±0.5 nm *(sponges)*	12.1±0.5 nm *(polymersomes and hexosomes)*
PEG_{45}-*b*-$PTPEMA_{42}$	11.7±0.5 nm *(cubosomes)*	13.2±1.0 nm *(hexosomes)*
PEG_{45}-*b*- $PTPEMA_{122}$	13.2±1.0 nm *(hexosomes)*	-

[a] Thickness measured from the FWHM of the electronic density profile perpendicular to the bilayer membrane through statistical analysis of about 30 different assemblies in the cryo-EM images.

Table S3. Solubility Parameters of the Binary Solvents.

$v_{THF}/(v_{THF} + v_{dioxane})$	**Solubility Parameters of the Mixed Solvents ($MPa^{-1/2}$)**
0%	20.5
25 %	20.1
40%	19.7
50 %	19.5
100%	18.6

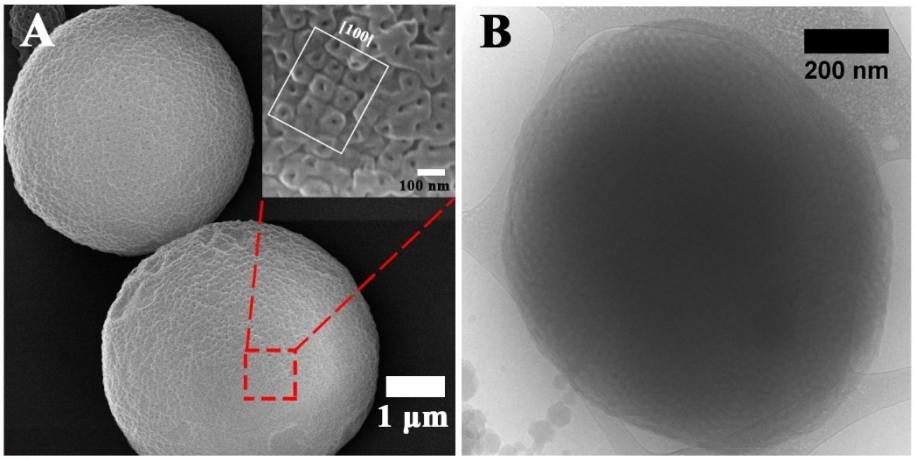

Figure S14. The SEM (A) and cryo-EM (B) images of PEG_{45}-*b*-$PTPEMA_{42}$ cubosomes formed in dioxane/THF/water system with THF content of 25%.

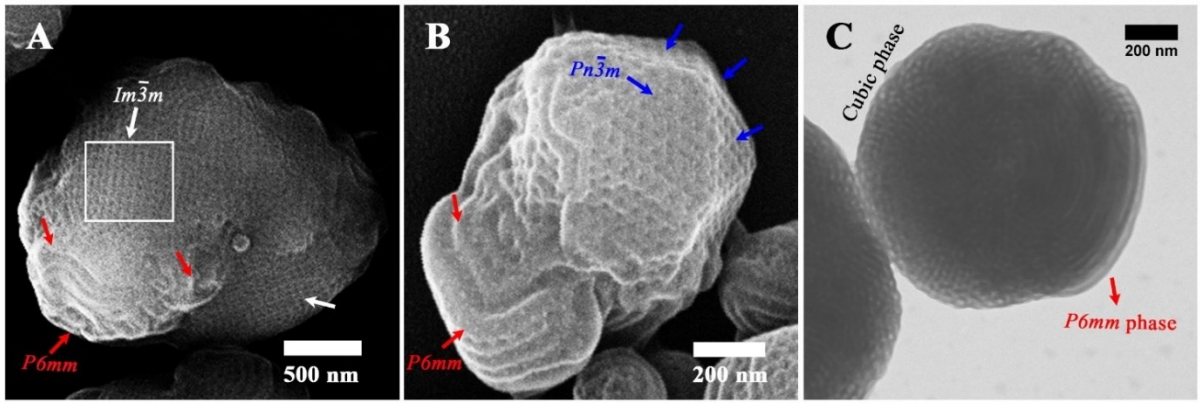

Figure S15. The SEM (A-B) and cryo-EM (C) images of PEG_{45}-*b*-$PTPEMA_{42}$ aggregates formed in dioxane/THF/water system with THF content of 40%. (A) The intermediate morphologies composed of $Im\bar{3}m$ and *P6mm* structures. The tetragonal pores (in white rectangle) correspond to $Im\bar{3}m$ structure, while the cylindrical channels (the red arrows) ascribe to *p6mm* structure. (B) The intermediate morphologies composed of $Pn\bar{3}m$ and *P6mm* structures. The polyhedral surfaces (the blue arrows) are the characteristic of $Pn\bar{3}m$ cubosomes. The cylindrical channels (the red arrows) belong to *p6mm* structure. (C) The intermediate morphologies showing the cubic and *P6mm* phase.

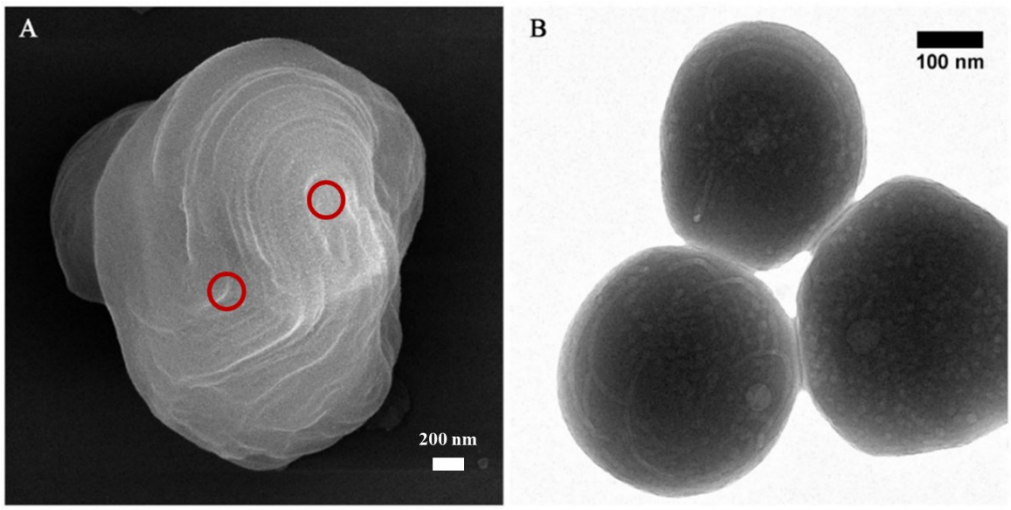

Figure S16. The SEM (A) and TEM (B) images of PEG_{45}-*b*-$PTPEMA_{42}$ hexosomes in dioxane/THF/water system with THF content of 50%. Red circles in A are used to highlight the two topological defects in surface of hexosomes.

6. SAXS data analyses

The scattering signal of powder samples is the sum of two contributions:

- A huge scattering from interfaces between the powder grains and the air, which is generally decreasing in q^{-4} (Porod law).
- Bragg peaks arising from the ordered structure inside the grains (Bragg law).

For the three samples measured by SAXS, the fits of the signal of interfaces are $q^{-3.2 \pm 0.2}$ variations. Such deviation from the Porod law often occurs due to the scattering by rough interfaces. After subtraction of this signal, the Bragg peaks are more visible and easier to fit using Lorentzian function. Thus, besides the Bragg angles of the various peaks which give the structure and the lattice parameter of the ordered structure, the Bragg peaks were fitted and their full (or half) width at half maximum (FWHM or HWHM) were obtained to estimate the sizes of the perfect crystallite (monocrystal) parts with cubic or hexagonal phase in the colloidal grains, using the Scherrer formula:

$$T_{cryst.} = \frac{K.\lambda}{\beta cos(\theta_B)}$$

where $T_{cryst.}$ is the size of the monocrystals in the grains or also called the correlation length of cubic or hexagonal structures, θ_B *the Bragg angle*, λ the wavelength of X-rays. K is a parameter, which depends on the structure and on the shape of the ordered objects. β is the FWHM of the Bragg peak (in radians), calculated from

$$\beta = \sqrt{{\beta_{FWHM}}^2 - {\beta_0}^2}$$

where β_0 is the FWHM of the incident X-ray beam and β_{FWHM} the FWHM of the Bragg peak. All parameters and results are listed in Table S4.

As for PEG_{45}-*b*-$PTPEMA_{42}$ cubosomes in dioxane (B), the first peaks (110) and (200) of were not visible enough in whole shape to do the fit, while the 3rd peak peak (440) may superpose with other signals in the high q range. Therefore, the correlation length of cubic structure of PEG_{45}-*b*-$PTPEMA_{42}$ cubosomes in dioxane was not calculated.

Table S4. Parameters of the Bragg peaks allowing the calculation of the sizes of crystallites $T_{cryst.}$ using the Scherrer formula. $\lambda = 0.1541nm$; β_0=0.008°; K is set to 1 (an approximated value usually taken).

Sample name	Co-solvent	q_B (nm^{-1})	θ_B (°)	FWHM (nm^{-1})	β_{FWHM} (°)	$T_{cryst.}$ (nm)
PEG_{45}-*b*-$PTPEMA_{122}$	Dioxane	0.287	0.403	0.103	0.072	120
PEG_{45}-*b*-$PTPEMA_{42}$	THF	0.225	0.316	0.118	0.083	110

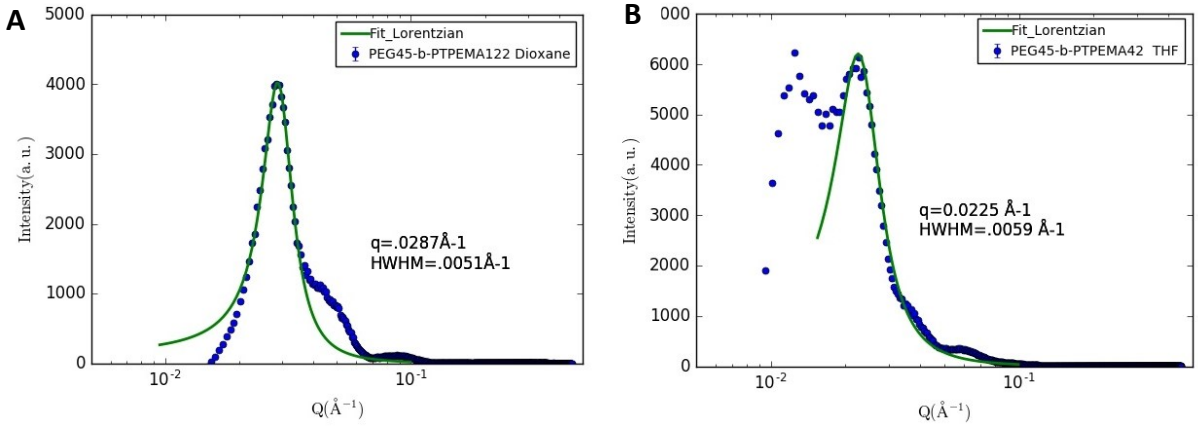

Figure S17. X-ray scattering profiles (dots) of PEG_{45}-*b*-$PTPEMA_{122}$ hexosomes in dioxane (A), and of PEG_{45}-*b*-$PTPEMA_{42}$ hexosomes in THF (B), after subtraction of a $q^{-3.2 \pm 0.2}$ variation due to the scattering from interfaces between colloids and air. Lines are fits of the peak with a Lorentz function using SasView software (M. Doucet et al. SasView Version 4.1, Zenodo, 10.5281/zenodo.438138.) The peak position and the half width at half maximum (HWHM) obtained is listed in Table S4.

7. Fluorescence characteristics of PEG-*b*-PTPEMA self-assemblies

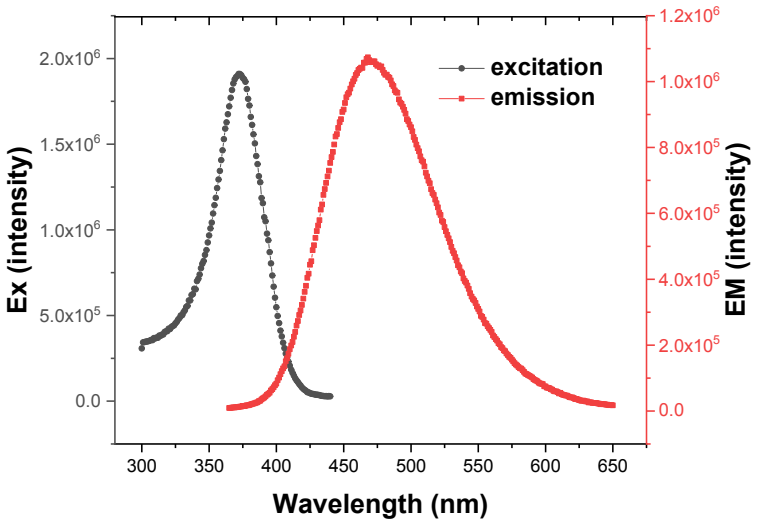

Figure S18. The excitation (grey) and emission (red) spectra of the PEG_{45}-*b*-$PTPEMA_{42}$ cubosomes. (Concentration: about 0.2 mg. ml^{-1}, excitation: 370 nm).

Measurement of fluorescent quantum yield (QY)

The absolute fluorescent quantum yields of the nanoparticles were measured by integrated sphere on a QM-40 spectrofluorometer (PTI, Horiba) equipped with a 150 W xenon lamp. The excitation wavelength was set as 360 nm, and QY measurement was repeated for three times for each sample.

8. Biocompatibility of PEG_{45}-*b*-$PTPEMA_n$ self-assemblies

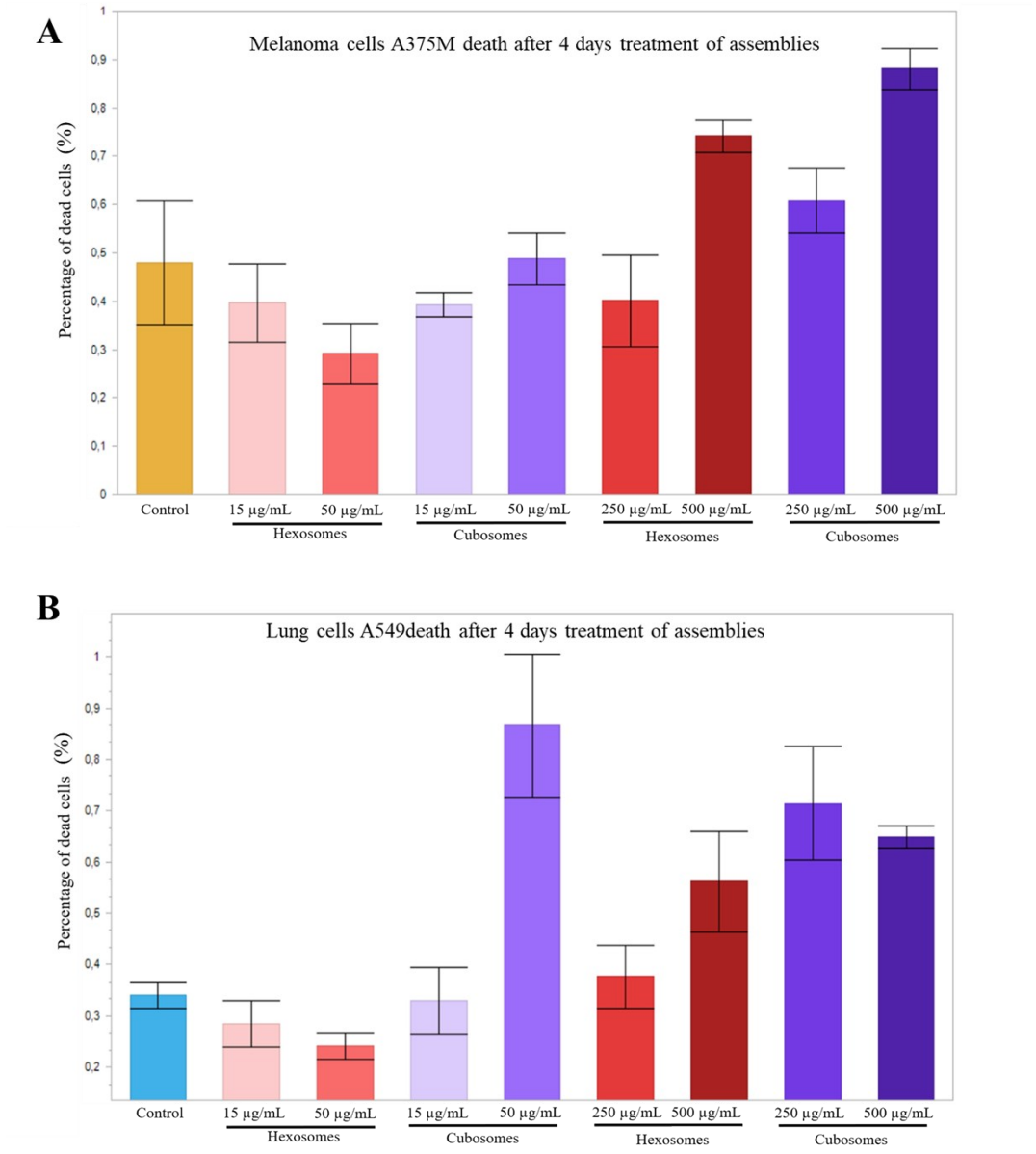

Figure S19. Toxicity of PEG_{45}-*b*-$PTPEMA_{42}$ cubosomes and PEG_{45}-*b*-$PTPEMA_{122}$ hexosomes on adherent cells. The plots show the percentage of dead cells for each culture condition, in presence or absence of PEG_{45}-*b*-$PTPEMA_n$ self-assemblies. (A) Melanoma cell death after four days of colloids treatment. (B) Lung cells death after four days of colloids treatment.

For melanoma cells A375M, the percentage of dead cells ranged between 0.3% and 0.9% after four days of incubation with PEG_{45}-*b*-$PTPEMA_{42}$ cubosomes. For lung cells A549, the percentage of dead cells ranged between 0.2% and 0.9% after four days of incubation with PEG_{45}-*b*-$PTPEMA_{42}$ assemblies. In both cell lines tests, there are very small variations in the

proportion of dead cells in the cells treated with PEG_{45}-*b*-$PTPEMA_n$ assemblies, which is similar to that of control cells for all tested conditions. All PEG_{45}-*b*-$PTPEMA_n$ cubosomes and hexosomes studied are therefore non-cytotoxic, indicating their excellent biocompatibility.

Figure S20 shows that the confluence and shape of cells treated with the PEG_{45}-*b*-$PTPEMA_{42}$ assemblies are similar to those of the control. In the background of cells treated with hexosomes or cubosomes, some spherical structures are visible (white arrows). These correspond to large colloids, which are particularly visible in the 250µg/mL and 500µg/mL conditions. The cell which are supposedly dead are colored in red. Note that some large cubosomes are also colored in red, meaning that they could be assimilated to dead cells.

Effectively, in the case of cubosomes the cell death is slightly higher than that of control and that in the case of hexosomes. This can be explained by the fact that the large particles in cubosome solution were counted as dead cells by the IncuCyte software. The hexosome solution also contains some large particles, however they were not (or less) counted as dead cells. This difference may be caused by the different interactions between PI and particles: PI might enter more easily into porous structures of cubosomes than into those of hexosomes. PI located in the nanopores of cubosmoes might have their intramolecular mobility restricted and fluorescence enhanced like PI bound to DNA.

Figure S20. Cell culture in presence of polymer assemblies. The pictures are bright field images collected after four days of treatment with assemblies.